

Hair Bundle Heights in the Utricle: Differences Between Macular Locations and Hair Cell Types

Jingbing Xue and E. H. Peterson

JN 95:171-186, 2006. First published Sep 21, 2005; doi:10.1152/jn.00800.2005

You might find this additional information useful...

Supplemental material for this article can be found at:

<http://jn.physiology.org/cgi/content/full/00800.2005/DC1>

This article cites 48 articles, 13 of which you can access free at:

<http://jn.physiology.org/cgi/content/full/95/1/171#BIBL>

Updated information and services including high-resolution figures, can be found at:

<http://jn.physiology.org/cgi/content/full/95/1/171>

Additional material and information about *Journal of Neurophysiology* can be found at:

<http://www.the-aps.org/publications/jn>

This information is current as of December 9, 2005 .

Hair Bundle Heights in the Utricle: Differences Between Macular Locations and Hair Cell Types

Jingbing Xue and E. H. Peterson

Department of Biological Sciences and Neuroscience Program, Ohio University, Athens, Ohio

Submitted 28 July 2005; accepted in final form 19 September 2005

Xue, Jingbing and E. H. Peterson. Hair bundle heights in the utricle: differences between macular locations and hair cell types. *J Neurophysiol* 95: 171–186, 2006. First published September 21, 2005; doi:10.1152/jn.00800.2005. Hair bundle structure is a major determinant of bundle mechanics and thus of a hair cell's ability to encode sound and head movement stimuli. Little quantitative information about bundle structure is available for vestibular organs. Here we characterize hair bundle heights in the utricle of a turtle, *Trachemys scripta*. We visualized bundles from the side using confocal images of utricular slices. We measured kinocilia and stereocilia heights and array length (distance from tall to short end of bundle), and we calculated a KS ratio (kinocilium height/height of the tallest stereocilia) and bundle slope (height fall-off from tall to short end of bundle). To ensure that our measurements reflect *in vivo* dimensions as closely as possible, we used fixed but undehydrated utricular slices, and we measured heights in three dimensions by tracing kinocilia and stereocilia through adjacent confocal sections. Bundle heights vary significantly with position on the utricular macula and with hair cell type. Type II hair cells are found throughout the macula. We identified four subgroups that differ in bundle structure: zone 1 (lateral extrastriola), striolar zone 2, striolar zone 3, and zone 4 (medial extrastriola). Type I hair cells are confined to striolar zone 3. They have taller stereocilia, longer arrays, lower KS ratios, and steeper slopes than do neighboring (zone 3) type II bundles. Models and experiments suggest that these location- and type-specific differences in bundle heights will yield parallel variations in bundle mechanics. Our data also raise the possibility that differences in bundle structure and mechanics will help explain location- and type-specific differences in the physiological profiles of utricular afferents, which have been reported in frogs and mammals.

INTRODUCTION

The diversity of behaviors required for survival means that each organism must exhibit a range of head movement velocities, accelerations, and frequencies. These head movements are inherently destabilizing. Yet vertebrates can compensate, apparently seamlessly, for such perturbations. How is detection and compensation matched to these constantly changing head movements?

A major advance in our understanding of this issue was the discovery that vestibular afferents, the neurons that relay hair cell signals to the brain, are physiologically heterogeneous (reviews: Goldberg 2000; Lysakowski and Goldberg 2004). This discovery raised the possibility that different afferent types might somehow encode head movements with different temporal characteristics (reviews: Eatock and Lysakowski 2005; Peterson 1998). For example, afferent responses to stimuli of differing intensities suggests that sensitive bouton

afferents terminating near the center of the turtle posterior canal are well suited to monitor subtle postural adjustments, whereas less sensitive calyx-bearing afferents are more likely to signal rapid head movements (Brichta and Goldberg 2000b).

Considerable attention has been focused on possible sources of afferent diversity including macro- and micro-mechanics (review: Rabbitt et al. 2004), diversity in hair cell transmitters (review: Highstein et al. 2005), and hair cell (review: Eatock and Lysakowski 2005) and afferent (review: Lysakowski and Goldberg 2004) biophysics. Much of this work has been inspired by the observation that physiological diversity in afferents is often strongly correlated with the morphology and spatial location of afferent terminals on the surface of the neuroepithelium. For example, afferents that enclose all their presynaptic hair cells in cup-like, calyceal endings (pure calyx afferents) differ, on average (i.e., averaged across epithelial loci), from afferents that include bouton endings in their terminals (dimorphs) or from pure bouton afferents (canals: Baird et al. 1988; Schessel et al. 1991; otolith organs: Goldberg et al. 1990). This suggests that hair cells contacting calyces (type I hair cells) and hair cells contacting boutons (type II hair cells) may have distinctive properties that contribute to diversity in their postsynaptic afferents. A second source of afferent diversity is suggested by observations that several physiological properties of afferents (e.g., discharge regularity, response dynamics, and rate intensity functions) vary with epithelial locus, even for the same afferent type (canals: Boyle et al. 1991; Brichta and Goldberg 2000a,b; Honrubia et al. 1989; O'Leary et al. 1976; otolith organs: Baird and Lewis 1986; Goldberg et al. 1990). This raises the question of whether there are comparable spatial patterns in hair cell properties that might help account for physiological differences between afferents.

One feature of vestibular receptors that is known to be markedly heterogeneous is the hair bundle: the ordered array of stereocilia that, together with the kinocilium, extend from the hair cell's apical surface. Bundles link extracellular events within the inner ear (forces set up by head movements) to the intracellular cascade that alters transmitter release from the hair cell and afferent firing. Thus these mechanoreceptive organelles are critical for hair cell signaling. It would be useful to know how functionally significant features of these bundles vary with hair cell type and with position on the sensory epithelium because this might help us understand the origins of type- and location-specific diversity in vestibular afferents and, perhaps, the origins of any afferent "tuning" to different

Address for reprint requests and other correspondence: E. H. Peterson, Dept. Biological Sciences, Irvine Hall, Ohio University, Athens, OH 45701 (E-mail: peterson@ohio.edu).

The costs of publication of this article were defrayed in part by the payment of page charges. The article must therefore be hereby marked "advertisement" in accordance with 18 U.S.C. Section 1734 solely to indicate this fact.

temporal characteristics of head movement. Unfortunately, there have been few quantitative descriptions of hair bundle structure and even fewer that describe quantitative variations in vestibular bundle structure as a function of epithelial locus or hair-cell type (see DISCUSSION).

Here we address this issue by describing spatial- and type-specific variation in bundle heights. We focus on bundle heights because experiments and models suggest that the heights of kinocilia and stereocilia affect several aspects of hair cell performance including frequency selectivity, linear operating range, sensitivity, stiffness, and perhaps response phase. Thus bundle heights have important consequences for a hair cell's ability to detect and encode head movements. Our major finding is that there are significant differences in bundle heights at different regions of the utricular macula that parallel known physiological differences between utricular afferents (frog: Baird and Lewis 1986; chinchilla: Goldberg et al. 1990). We also report that type I and type II hair cells differ significantly from each other in bundle heights. Some of these data have appeared previously in abstract form (Xue and Peterson 2004).

METHODS

Four juvenile turtles, *Trachemys (Pseudemys) scripta elegans*, of both sexes (4.75 to 5.25 in carapace length; Kona Scientific, Germantown, WI) provided useful data on bundle heights. We used two additional animals for utricular whole mounts (Fig. 1). Animal care protocols have been published previously (Brichta and Peterson 1994). All animals were killed via an overdose of Euthasol (390 mg pentobarbital sodium and 50 mg phenytoin sodium per ml; 0.5 ml im). We followed the Ohio University Animal Care and Use Committee guidelines in all experiments.

Utriclar whole mounts

For utricles visualized as whole mounts (Fig. 1), we excised the utricular macula and surrounding epithelia from the membranous labyrinth, secured it in a silicone elastomer (Sylgard)-lined dish with minuten insect pins (Fine Science Tools), removed the connective tissue falx that overlies the lateral macula (Fig. 2A), and removed the otolithic membranes using a fine stream of bath solution. The utricle shown in Fig. 1A was used to examine the otoconial membrane for another study, so all procedures (fixation, dissection, staining) were conducted in artificial endolymph (Crawford et al. 1991) to minimize distortion of the otolithic membranes (Freeman et al. 1993).

Utriclar slices

For utricles visualized as slices (Fig. 2), we decapitated killed turtles, bisected the heads, and removed the half-brains, leaving the labyrinth and a stump of cranial nerve VIII (CN8) intact. We labeled afferents using Micro-Ruby (BDA/Rhodamine 3000MW; Molecular Probes D-7162; 33 mg/ml in distilled water), fixed utricles after 4–6 h in 10% buffered formalin phosphate (Fisher), embedded them in 4% low melting point agarose, and sliced them at 60 μ m using a Leica VT 1000S vibrating blade microtome. After sectioning, we stained the slices to visualize kinocilia and stereocilia as follows. To visualize kinocilia, we applied a blocking solution (5% fetal calf serum, 1% bovine serum albumin, 0.1% DMSO) to the slices for 1 h at room temperature followed by a monoclonal antibody against acetylated α -tubulin (Sigma T6793; diluted 1:1,000 in blocking solution) for 48 h at 4°C. Then we rinsed the slices in blocking solution (3 changes, 1 h each) and incubated them in secondary antibody conjugated to Alexa-Fluor 488 (Molecular Probes A-11001, diluted 1:200 in blocking solution) for 1 h at room temperature. Finally, we rinsed the slices (3 changes, 1 h each) and visualized stereocilia by applying phalloidin conjugated to Alexa-Fluor 633 (Molecular Probes A-22284, diluted 5 U/ml) for 30 min at room temperature, followed by a final rinse (3 changes, 5 min each). Steps following fixation (e.g., dissection, staining) were conducted in either artificial endolymph (for comparison with utricles used to study the otoconial membrane) or 0.1 M phosphate buffer; we observed no quantitative differences in bundle heights between these two postfixation bathing media.

Identification of type I hair cells

One goal of the present study was to learn whether type I and type II hair cells differ in bundle heights. Thus it was necessary to visualize calyceal terminals, which define hair cell type. To do this, we applied a small pellet of gelfoam that had been infiltrated with Micro-Ruby to the exposed stump of CN8, covered it with a drop of cyanoacrylate adhesive (Loctite 404, Henkel Technologies), and maintained the half head in circulating, oxygenated turtle Ringer solution (Hounsgaard and Nicholson 1990). After 4–6 h, we fixed the utricles as described in the preceding text (see *Utriclar slices*), and we examined labeled utricles as whole mounts (Fig. 1B) or slices (Fig. 2).

Confocal microscopy

We visualized utricles using a Zeiss LSM 510 confocal microscope. To scan utricular whole mounts (Fig. 1), we used a $\times 10$ objective (NA = 0.30) and single-track scanning with a 488 nm laser line for α -tubulin (kinocilium label), a 543 nm laser line for MicroRuby

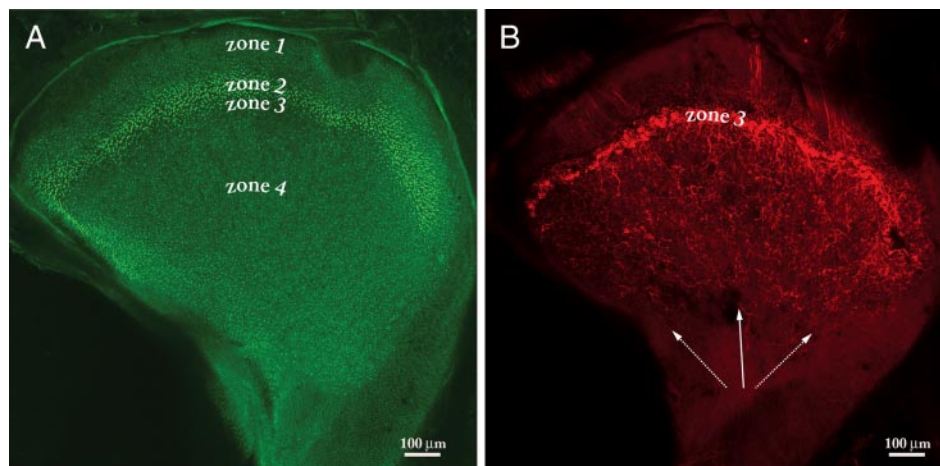


FIG. 1. Turtle utricular whole mounts. Confocal projections of left utricle; anterior is to the right. *A*: we stained this utricle with phalloidin, a probe for filamentous actin, to visualize bundles. The striola is visible as a crescent-shaped band of bright bundles. We divided the macula into 4 zones based on bundle structure and afferent innervation. Zones 1 and 4 correspond to the lateral and medial extrastriola, respectively. Zones 2 and 3 are parallel bands that form the striola. Type I hair cells are restricted to zone 3. *B*: we labeled afferents with Micro-Ruby. The crescent-shaped band of calyces defines zone 3. Solid arrow: orientation of the primary transect. Dotted arrows: orientation of radial transects through the posterior (left) and anterior (right) margins of the striola.

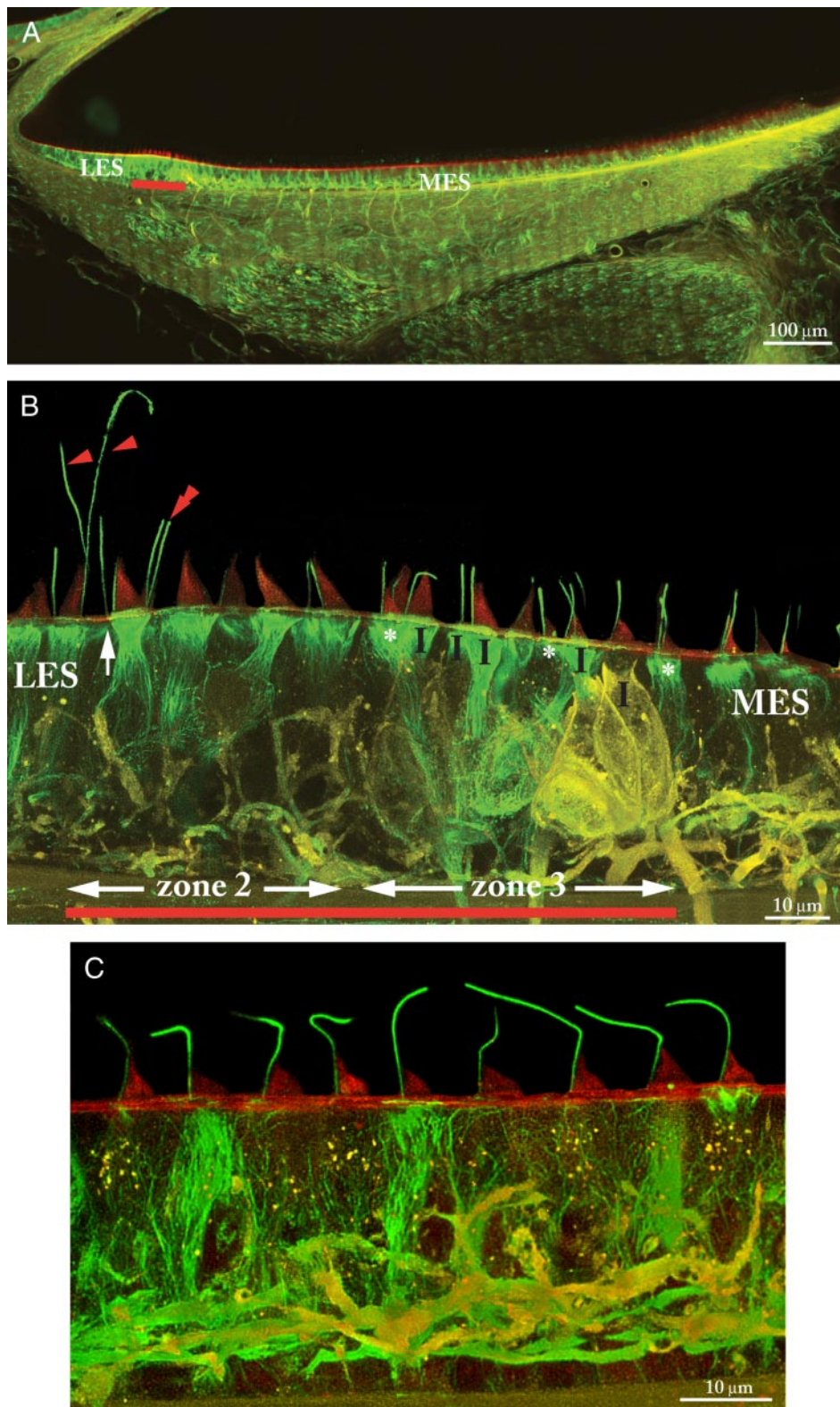


FIG. 2. Utricular slices. These confocal images are from slices aligned with the primary transect. Afferents are labeled with Micro-Ruby (yellow); stereocilia are labeled with phalloidin (red); and kinocilia are labeled with an antibody against acetylated α -tubulin (green). LES, lateral extrastriola; MES, medial extrastriola; Red bar, striola. The images in *B* and *C* were enhanced using deconvolution (Autoquant). *A*: low-magnification view of the primary transect. Large bundles of the striola are visible. The connective tissue falx that overlies the lateral macula is at upper left. *B*: higher-magnification image of the striola and adjacent LES and MES. Utricular kinocilia have uniform dimensions along their lengths; we saw no bulbed kinocilia. The distal regions of some kinocilia appear expanded because they are more brightly stained than the kinocilial bases; the reason for this irregular staining is unclear. Type I hair cells in striolar zone 3 are labeled (I). Two type I hair cells at right contact strongly labeled calyces. The left-most type I cell contacts a calyx that is more weakly labeled but clearly distinguishable in the original confocal image. The somata and calyces of the remaining type I hair cells (2nd and 3rd from left) are partially displaced from the plane of the confocal image. All other hair cells are type II. Some LES bundles just lateral to the line of polarity reversal (LPR; arrow) have the longest kinocilia in the utricle (arrowheads). Two LES hair cells with very long kinocilia (double arrowhead) appear to be medial to the LPR because the LPR follows an irregular trajectory. Note the gradual change in bundle structure from the LPR to the medial extrastriola. In zone 2, kinocilia and the tallest stereocilia are the same height (KS ratio ~ 1). Within zone 3, kinocilium height is approximately the same as in zone 2 bundles, but the height of the tallest stereocilia gradually decreases toward the MES, which increases the KS ratio. At each point within zone 3, type I bundles have lower KS ratios than adjacent type II bundles (asterisks). *C*: high-magnification image of bundles in the medial extrastriola. Note that bundles in this region are more homogeneous than those in the striola (*B*). These type II hair cells are distinctive because their bundles have very high KS ratios and shallow slopes.

(afferent label), and a 633 laser line for phalloidin (stereocilia label). To measure bundle heights from a utricular slice (e.g., Fig. 2), we collected a series of high magnification stacks from lateral to medial margins of the utricle; each stack overlapped its neighbors slightly so that we could construct a high magnification montage of the entire slice. We collected each stack using an Alpha Plan-Fluar $\times 100$ oil-immersion objective (NA = 1.45) and multi-track scanning with

488, 543, and 633 nm laser lines as described in the preceding text. In the resulting images, kinocilia are pseudo-colored green, afferents appear yellow, and stereocilia appear red (Fig. 2, *B* and *C*). We used a $0.5 \mu\text{m}$ z -axis step size, and we scanned only the most superficial 25–40 μm of the slice (50–80 optical sections per stack); at deeper levels, we could not visualize bundles clearly enough for accurate measurements.

Quantification of bundle heights

Measurements made from micrographs will generally underestimate bundle heights because of image foreshortening; this occurs when the z dimension is collapsed onto a single xy plane. To achieve greater accuracy, we measured features of interest in three-dimensional space. We used the NeuroLucida computerized morphometry system (Microbrightfield), equipped with a confocal module, which allowed us to trace features of interest through multiple optical sections. This approach had two advantages; it allowed us to measure heights of curved processes (kinocilia and stereocilia) and to preserve z-axis information, thereby minimizing measurement errors due to foreshortening. We measured the following features of each bundle (Fig. 3): kinocilium height, height of the tallest and shortest stereocilia, and array length (distance from the tallest to the shortest stereocilia), and we used these measurements to calculate a KS ratio and a slope for each bundle. In addition to measuring features of the bundle, we measured the distance of each bundle from the line of polarity reversal; the tall ends of utricular bundles face each other across this reversal line. Finally, we assigned each bundle to its hair cell type based on the presence or absence of a calyx surrounding the hair cell soma (Fig. 2B).

Data analysis

Our primary data on bundle heights are from two utricles (different turtles). Utricular slices from both turtles were cut parallel to a line running from the entrance of the utricular nerve to a point approximately mid-way between the anterior and horizontal cristae (Fig. 1B, solid arrow). All bundles along this primary transect have approximately the same activation (excitation/inhibition) axes; their polarities depend on whether they are medial or lateral to the reversal line. For each turtle, we examined four consecutive slices, and we measured all hair bundles in these slices that could be visualized clearly. Of 1,795 hair cells in these slices, we measured all features of interest (Fig. 3) on 805 bundles (44.8%); quantitative data from the 805 bundles are

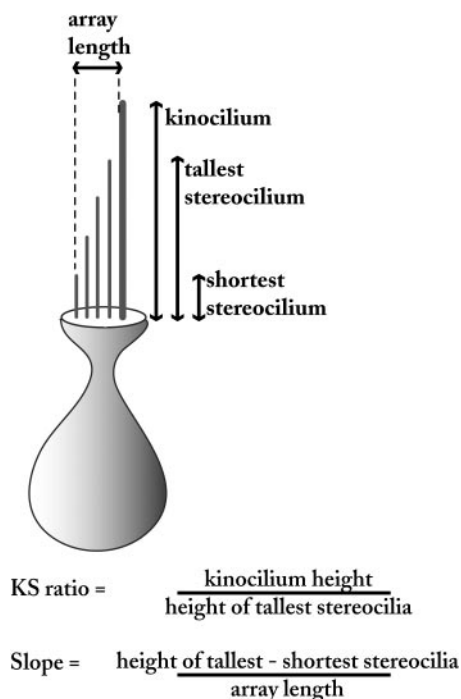


FIG. 3. Bundle measurements. We measured heights of kinocilia and the tallest and shortest stereocilia and array length (distance from the tallest to the shortest stereocilia, measured parallel to the hair cell's apical surface). We used these measurements to calculate a KS ratio and a slope for each bundle.

illustrated in Figs. 4, 5A, 6, and 7. Exploratory and inferential statistical analyses were implemented in Statistica (ver. 6.1; StatSoft) or S^+ (ver. 6.2; Insightful). Our data presented challenges for statistical analysis because some variable distributions were markedly non-normal. Accordingly, we used robust statistics for our analyses because they make the fewest assumptions about underlying variable distributions while often providing more power than nonparametric methods (Wilcox 2005). We implemented all robust functions in S^+ . To compare bundles at different locations on the macula we used *tIway* (analog of 1-way ANOVA) and *lincon* (for multiple comparisons) (Wilcox 2005; chapt. 7). To compare overall differences in bundles of type I and type II hair cells, we used *ks* (Kolmogorov-Smirnov test) (Wilcox 2005; section 5.1). To compare differences between cases or hair cell types while controlling for effects of location, we used *ANCOVA* (a robust analysis of covariance, with location as the covariate) (Wilcox 2005; section 11.8). To describe spatial gradients in and near the striola (Figs. 6 and 8), we used MM linear regression (available in S^+). We summarized spatial trends across the macula (Fig. 4) using Loess fits. This method of smoothing uses a series of weighted, local regressions to capture patterns in bivariate data that cannot be fit with simple linear or quadratic equations (Cleveland 1993). For the fits in Fig. 4, we used a local quadratic fit (because there are local maxima and minima in our data), a Gaussian weighting function, and a span (which determines the degree of smoothing) of 0.3. We implemented Loess fits in S^+ .

To ensure that our results are not unique to the primary (central) transect described above, we made less extensive measurements of bundle heights along two additional radial transects. They extended from the entrance of the utricular nerve to the posterior or anterior margins of the striola (Fig. 1B, dotted arrows). For these posterior and anterior transects, we measured bundles along the full lateral to medial extent of the macula in one slice, and we measured bundles in the lateral extra-striola, striola, and adjacent medial extrastriola ($\leq 200 \mu\text{m}$ medial to the line of polarity reversal) of additional slices because bundle structure in this region is markedly heterogeneous. Table 1 summarizes our data base for height measurements; the marked difference in sample sizes from different zones of the utricle reflects differences in zone size (Fig. 1A). Tables 2–7 summarize bundle measurements for primary, posterior, and anterior transects. Summary statistics for individual animals are presented in *Supplemental material*.

SUPPLEMENTAL MATERIAL

Supplementary Tables 1–6¹ contain summary statistics on hair bundle heights for individual turtles. For completeness, summary data on primary, posterior, and anterior transects are also included.

RESULTS

In utricular wholemounts labeled with phalloidin, the approximate position of the striola is visible as a band of bright bundles (Fig. 1A). Striolar bundles are brighter than extrastriolar bundles because they are larger: they have more (zone 3) (Moravec and Peterson 2004) or thicker (zone 2) stereocilia. Micro-Ruby loading of utricular afferents revealed a narrow band of calyces that followed the trajectory of these bright bundles (Fig. 1B); this confirms earlier reports that type I hair cells in *T. scripta* are restricted to the striola (Jorgensen 1974, 1988; Severinsen et al. 2003). In utricular slices, the approximate position of the striola is visible as a region of large bundles; the neuroepithelium in this region (Fig. 2A, red bar) is thicker than in the extrastriola. In

¹ The Supplementary Material for this article (six tables) is available online at <http://jn.physiology.org/cgi/content/full/00800.2005/DCI>.

high-magnification images, hair cells can be assigned to one of four utricular zones (Figs. 1A and 2, B and C) (Moravec and Peterson 2004; Moravec et al. 2003; Peterson and Rowe 2001). Zone 1 corresponds to the lateral extrastriola (LES); it contains type II hair cells only. Zones 2 and 3 form the striola. Zone 2 is a band of type II hair cells just medial to the line of polarity reversal (LPR); it is 15–25 μm wide. Occasional bundles (<10 per transect) just lateral to the LPR have striolar-like structure (short kinocilia and low KS ratios), and preliminary calretinin immunocytochemistry suggests they may belong to zone 2 (i.e., they are calretinin-negative like hair cells in zone 2 and unlike other hair cells in zone 1) (Xue et al. 2005). In this study, we included them in zone 1 (LES), which will slightly decrease measured differences between zones 1 and 2. Zone 3 contains both type I and type II hair cells; it is ~ 50 μm wide. Zone 4 contains type II hair cells only; it corresponds to the medial extrastriola (MES). High-magnification images along the primary transect revealed three sources of variation in bundle dimensions: regional variation in type II bundles, regional variation in type I bundles, and differences between hair cell types.

Regional variation in type II hair bundles.

The dimensions of type II bundles in the primary transect vary systematically with utricular locus. The two turtles (*turtle 2*, *turtle 3*; see Supplementary material) exhibited similar spatial patterns. Figure 4 shows combined data for both turtles. The scatter plots (*left*) show how four measured (A, B, D, and E) and two calculated (C and F) variables change from lateral to medial across the macula. The box plots (*right*) summarize differences between zones. Curved lines in the scatter plots are Loess (local regression) (Cleveland 1993) fits for turtle 2 (—) and turtle 3 (····). We plot them separately because the two turtles showed small but statistically significant differences on some variables at some macular locations, typically in the far extrastriola. It is unlikely that these differences are biologically significant. Summary statistics for each zone and hair cell type are given in Tables 2–7. For data summaries of individual turtles, see Supplementary material.

Bundle heights (Fig. 4, A–D) reach local maxima or minima in zone 2: kinocilia are shorter and both the tallest and shortest stereocilia are taller than in any other region of the macula. The average KS ratio for zone 2 bundles is 0.996; thus kinocilia on these type II hair cells are approximately the same height as the tallest stereocilia in the same bundle. Array lengths (Fig. 4E) are shortest in the LES (zone 1: 2.6 ± 0.62 μm), intermediate in the striola (zones 2 and 3 combined: 3.2 ± 0.50 μm), and greatest in the MES (zone 4: 4.0 ± 0.68 μm). Bundle slope (Fig. 4F) is steepest for bundles just lateral to the line of polarity reversal and decreases systematically toward the medial and lateral margins of the macula. Bundles in the MES have especially long arrays and shallow slopes (Figs. 2C and 4, E and F).

Figure 5A illustrates how KS ratio and bundle slope covary. The relation between KS ratio and slope is nonlinear, and bundles in each zone occupy a characteristic position in the scatter plots. Note that type I bundles in zone 3 (green circles) are close to zone 2 bundles in this variable space, whereas type II bundles in zone 3 (green triangles) are closer to type II bundles in zone 4.

There is a significant effect of zone for all six variables (*t1way*: $P < 0.000003$ for all variables). Post hoc comparisons indicate that differences between zones are significant (*lincon*:

$P < 0.05$) for all comparisons with the following exceptions: 1) Kinocilium height is not different in zones 2 and 3 (Figs. 4A and 6A). 2) Heights of the tallest stereocilia in striolar zone 3 and the MES are not significantly different (Fig. 4B). 3) The shortest stereocilia are longest in zone 2 and not significantly different across the other three zones (Figs. 4D and 6D). 4) Array lengths are comparable in striolar zone 3 and the LES (Fig. 4E). And 5) average slopes do not differ significantly between striolar zone 2 and the LES, but slopes in the LES are markedly more heterogeneous (Fig. 4F).

Average differences between zones (Fig. 4, box plots) provide useful summaries of broad spatial patterns, but they do not adequately represent spatial gradients in bundle structure across the striola and adjacent extrastriola (Figs. 6 and 7). LES bundles (zone 1) are particularly heterogeneous (Fig. 6, A, B, and F). Within 30 μm of the line of polarity reversal, a few bundles (3–4%) resemble those in striolar zone 2: both their kinocilia and their tallest stereocilia are short. Other bundles on this narrow region have extremely tall kinocilia (>40 μm) and, in some cases, tall stereocilia (>20 μm); these bundles appear as “outliers” in the box plots of Fig. 4 (i.e., their values are $>1.5 \times$ interquartile range) (Emerson and Strenio 1983). Still further laterally, LES bundle heights are more homogeneous, resembling those of the MES.

Medial to the line of polarity reversal, type II bundle dimensions change gradually from zone 2, through zone 3, and into zone 4 (Figs. 4, 6, and 7). Within zone 3 alone, type II bundles show no significant dependence on macular locus for any variable, perhaps because sample sizes are small. Across the total striola (zones 2 and 3 combined), heights of the tallest and shortest stereocilia decline significantly with distance from the reversal line (Fig. 6, B and D) as does bundle slope (Fig. 6F); KS ratio increases (Figs. 6C and 7). For all variables except array length, lateral-to-medial spatial trends within the striola continue into the MES, and all variables reach approximately asymptotic values 150–200 μm medial to the line of polarity reversal (Fig. 4). Thus the dimensions of type II bundles vary markedly in and around the striola, but they are relatively uniform in more peripheral regions of the macula.

Regional variation in type I hair bundles

Type I hair cells are restricted to striolar zone 3, but within this narrow band their bundles are spatially heterogeneous (Figs. 6 and 7). Two variables, height of the tallest stereocilia (Fig. 6B) and KS ratio (Figs. 6C and 7), exhibit a significant dependence on distance from the reversal line. The height of the tallest stereocilia in the bundle decreases and, therefore, the KS ratio increases.

Differences between type I and type II bundles

There are significant structural differences between bundle types at the same macular locus. The box plots in Fig. 6 illustrate average differences between type I and type II bundles in zone 3. Confidence intervals are nonoverlapping for height of the tallest stereocilia, KS ratio, array length, and slope, suggesting that type I and type II hair cells differ significantly (Fig. 6B, C, E, and F). We confirmed this using a *ks* test (see *P* values accompanying box plots). Analysis of covariance (ANCOVA: with distance from the LPR as the covariate) reveals that at most positions within zone 3 there is a significant difference between type I and type II hair cells for

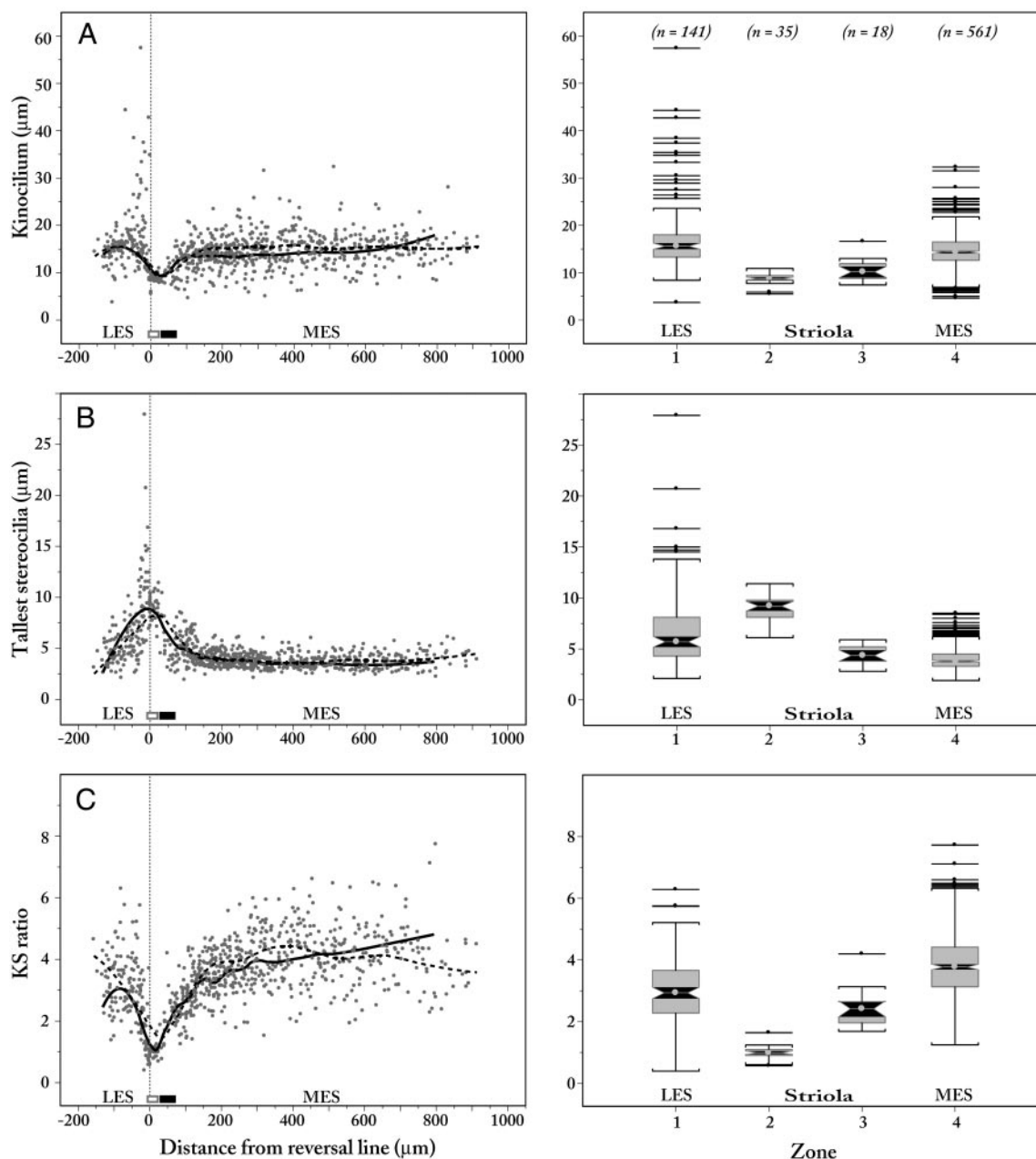


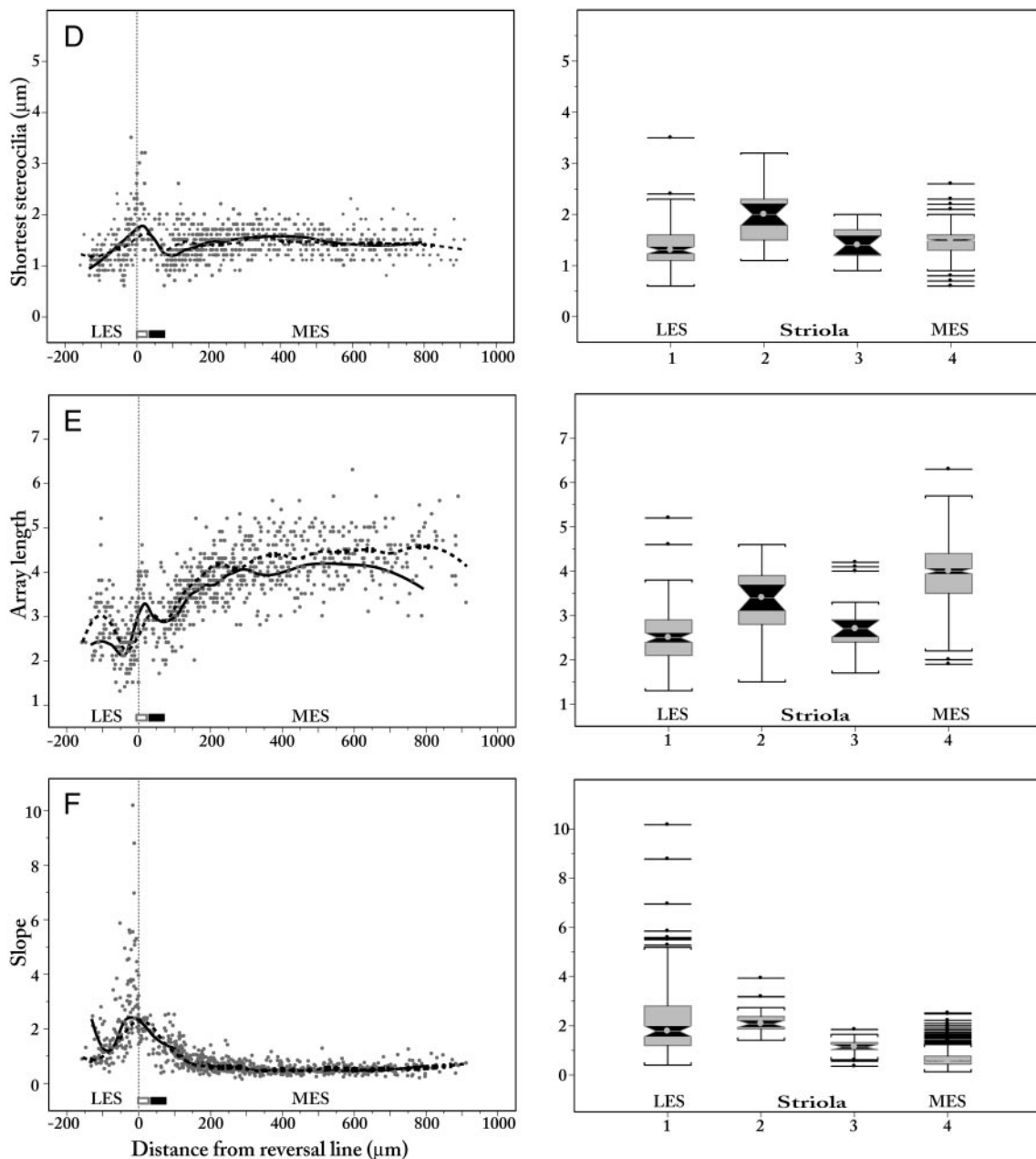
FIG. 4. Spatial variation in the structure of type II hair bundles. *Left:* scatter plots show how 4 measured (A, B, D, and E) and 2 calculated (C and F) variables change from lateral to medial along the primary transect. Each point represents 1 hair bundle. 0: line of polarity reversal. Bars just medial to the reversal line indicate the approximate position of the striola. □, striolar zone 2; ■, striolar zone 3. Lines are Loess fits for 2 different turtles (Table 1; Supplementary material). *Right:* box plots show average differences between type II hair bundles in the 4 zones. ○: median; □, interquartile range. ■, confidence intervals of the median. Nonoverlapping confidence regions suggest that differences between zones are significant. We confirmed this using robust analogues of a 1-way ANOVA and post hoc comparisons (see text). Whiskers: 1.5 × interquartile range. Isolated points: outliers.

the same four variables: the tallest stereocilia are taller on type I bundles than on type II bundles ($P < 0.01$), array lengths are longer ($P < 0.05$), KS ratios are lower ($P < 0.01$), and bundle slopes are more steep ($P < 0.05$). Figure 7 shows one example of these type- and location-specific differences within zone 3.

Posterior and anterior transects

Hair bundles from radial transects through posterior and anterior striola exhibit similar location- and type-specific variation as do bundles from the primary (central) transect

including 1) relatively homogeneous structure in the mid- to far- lateral and medial extrastriola, 2) characteristic spatial gradients in the striola and adjacent extrastriola for each variable, and 3) significant differences between type I and type II hair cells at the same macular locus for four variables: height of tallest stereocilia (ks test for posterior and anterior transects combined: $P = 2.5 \times 10^{-11}$), KS ratio ($P = 6.9 \times 10^{-8}$), array length ($P = 1.0 \times 10^{-9}$), and slope ($P = 0.0003$). This is illustrated for KS ratio and bundle slope in Figs. 5 and 8. Posterior and anterior transects differed from the primary transect in two ways. First, the

FIG. 4. *Continued*

shortest stereocilia on type I hair cells are significantly taller than on type II hair cells (*ks* test for anterior and posterior transects combined: $P = 0.0002$). Second, the dependence of type I KS ratios on position within zone 3 was not significant (Fig. 8) perhaps because sample size was small ($n = 18$ and $n = 20$, respectively, vs. $n = 50$ for the primary transect; Table 1). Data for posterior and anterior transects are summarized in Tables 2–7. Data for individual turtles are summarized in Supplementary material.

DISCUSSION

Our most important finding is that bundle heights differ significantly with macular location and hair cell type. Figure 9 summarizes these differences.

Dimensions of type II bundles do not vary with location in mid- to far-extrastriola. In contrast, type II bundle structure exhibits a marked dependence on macular locus in the striola and adjacent extrastriola. Some type II bundle dimensions appear to be more tightly constrained in and near the striola. For example, kinocilium height in the striola is less variable than in the MES; this suggests that coupling of type II kinocilia to the otoconial membrane of the striola may be more tightly controlled during development than coupling in the MES. Support for this suggestion comes from observations that kinocilia in the MES extend for variable distances into the thick ($\sim 100 \mu\text{m}$) otoconial layer, but kinocilia in the striola extend only to the gel layer of the otoconial membrane (unpublished data). The height at which a kinocilium enters the

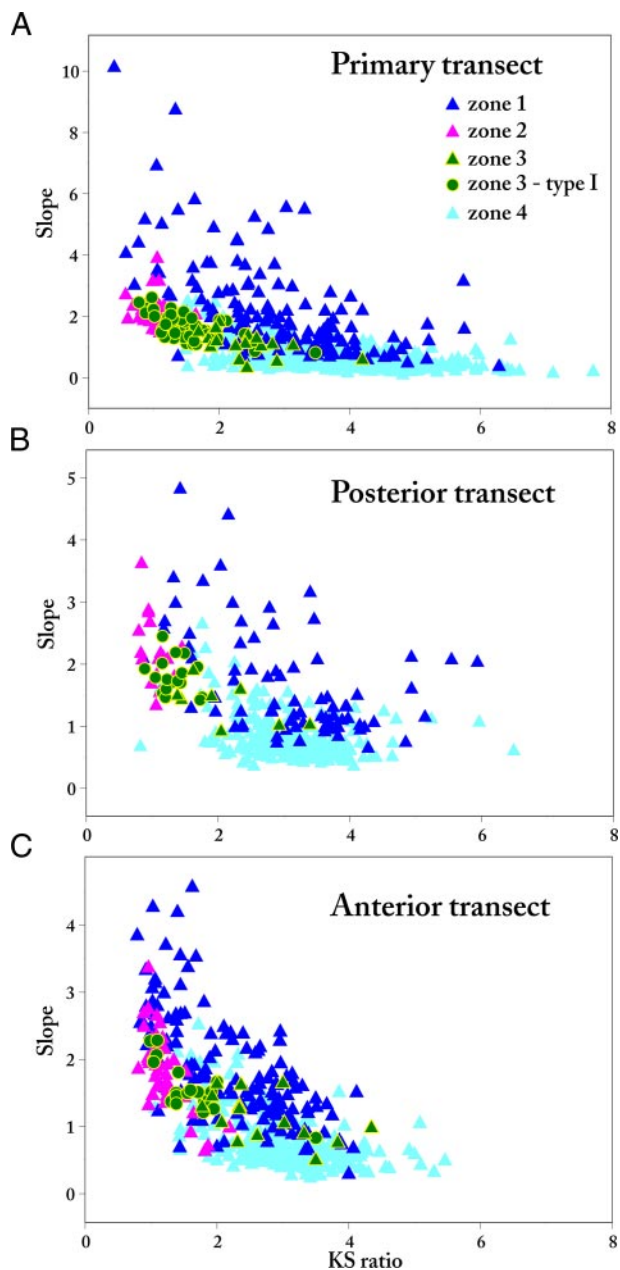


FIG. 5. Spatial- and type-specific variation in KS ratio and bundle slope. Scatter plots show how 2 calculated variables, KS ratio and bundle slope covary for the primary (A), posterior (B), and anterior (C) transects. Bundles in each zone occupy a characteristic position in this variable space. All 3 transects show the same basic pattern.

otoconial membrane is the effective point of force application. Thus this height, not kinocilium height per se, is important for hair bundle mechanics.

Our data on type II bundle heights reinforce our earlier suggestion (Moravec and Peterson 2004; Peterson and Rowe 2001) that the utricular striola can be subdivided into two bands based on bundle structure: zones 2 and 3. Zone 2 bundles are more homogeneous than those in zone 3, and they differ significantly from zone 3 bundles on all variables except kinocilium height (Fig. 4): stereocilia and array lengths are longer, KS ratios are lower, and bundle slopes are steeper. Thus zone 2 hair cells are highly specialized in structure and probably also in mechanics (see *Functional significance of*

bundle heights). Type II bundles in striolar zone 3 appear in some respects to be transitional between type II bundles in zones 2 and 4 (e.g., Fig. 7), but they are more similar to type II bundles in zone 4 than those in zone 2 (e.g., Fig. 5).

Type I bundles exhibit significant dependence on macular locus in the primary transect (Fig. 6): heights of the tallest stereocilia decline, and KS ratios increase systematically from lateral to medial within zone 3. In addition, type I bundles differ from type II bundles in the height of the tallest stereocilia, array length, KS ratio, and bundle slope. This is true whether one compares average dimensions of type I and II bundles within zone 3 (Fig. 6, box plots) or compares the two bundle types at comparable locations within zone 3 via analysis of covariance. Type I bundles also bear significantly more stereocilia than any type II bundles in the utricle (Moravec and Peterson 2004).

Methodological considerations

To demonstrate these location- and type-specific differences in bundle heights we needed to satisfy four criteria.

The first criterion is accurate measurements. They are essential for realistic models of hair bundle mechanics. We used two strategies to maximize the accuracy of our height measurements. First, we visualized kinocilia and stereocilia using different markers so we could clearly distinguish them. This is important for bundles in which kinocilia and the tallest stereocilia in the same bundle have similar lengths (KS ratio ~ 1). Second, we measured kinocilia and stereocilia lengths by tracing them in three dimensions using a computerized three-dimensional morphometry system. This allowed us to measure curving processes, e.g., tall kinocilia (e.g., Fig. 2C). It also enabled us to preserve z-axis information and so avoid underestimates of lengths due to foreshortening. Foreshortening can result in serious errors when measurements are made from scanning electron micrographs because the z dimension is collapsed onto an xy plane. This may help explain why a recent study of bundles in turtle utricle using scanning electron microscopy (Severinsen et al. 2003) reported shorter kinocilium heights (e.g., 5–7 μm in the striola) than when kinocilia are measured in three dimensions (9–11 μm) (Fontilla and Peterson 2000; present study). Shrinkage, which is significant in material prepared for scanning microscopy, may also have contributed to this difference.

Shrinkage due to fixation is also a potential source of error in the present study. We think significant shrinkage is unlikely for three reasons. First, fixation (unlike dehydration) produces no significant dimensional changes, even in highly hydrated tissues (Edge et al. 1998). Second, Fontilla and Peterson (2000) suggested that there is only 5–6% shrinkage of kinocilia in dehydrated tissue compared with DIC measurements from living bundles. Third, kinocilium heights in the present dehydrated material (e.g., median: 8.8 μm in zone 2) are nearly identical to those in live bundles (median 8.61 μm in zone 2) (Spoon et al. 2005). Thus kinocilia (and probably stereocilia) resist axial shrinkage, even in dehydrated material, perhaps due to their cytoskeletal cores. We conclude that bundle heights in the present study are within $<5\%$ of values that occur in vivo.

The second criterion is adequate sample size. One reason for the lack of quantitative information about bundle dimensions is the difficulty of collecting large enough samples for statistical

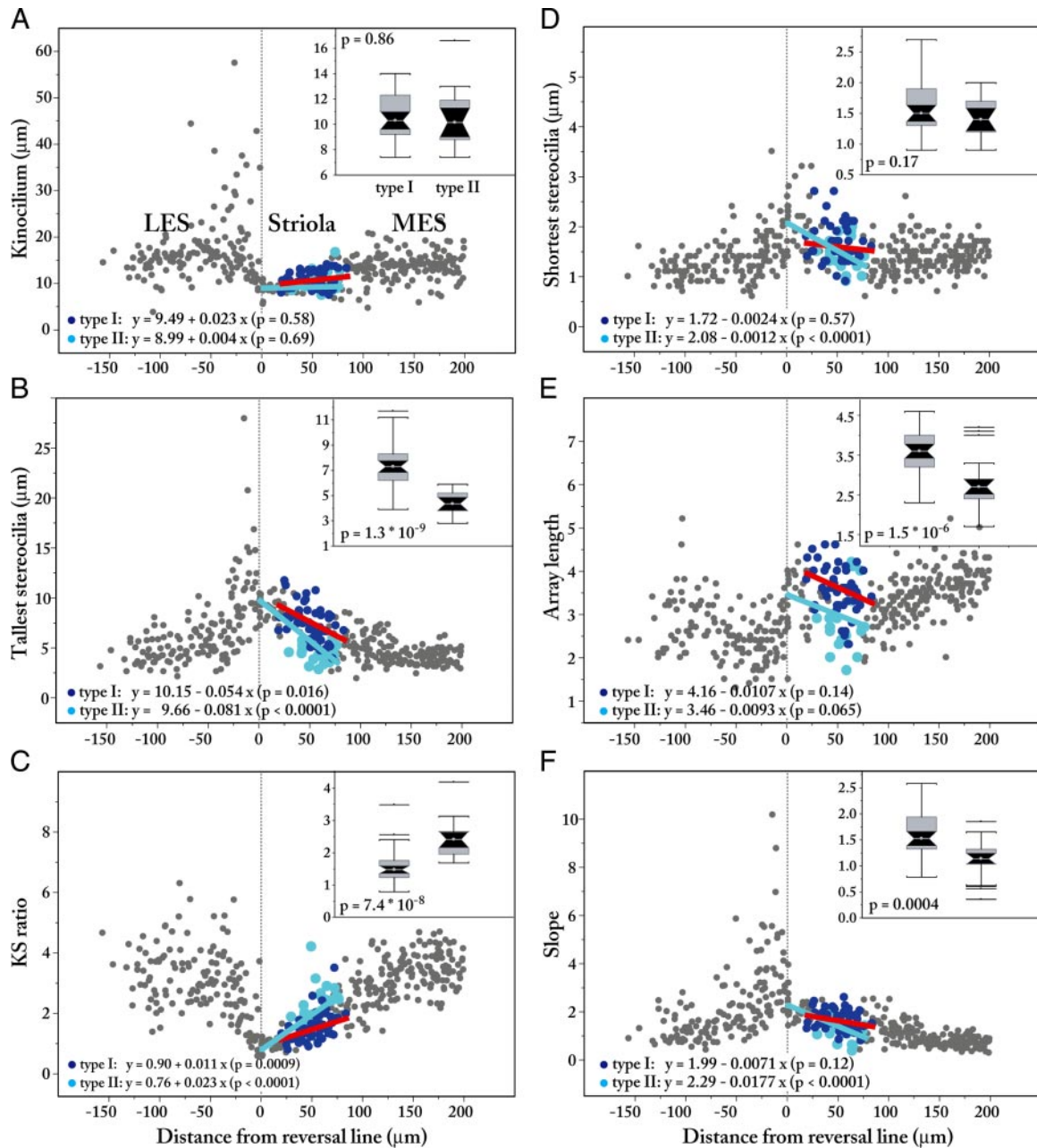


FIG. 6. Spatial- and type-specific variation in bundles of the striola and adjacent extrastriola. Scatter plots show details of bundle structure relative to the line of polarity reversal (0) for the LES, striola, and adjacent MES. These macular subdivisions are labeled in (A). Each symbol represents 1 hair bundle. Dark gray circles, bundles $\pm 200 \mu\text{m}$ from the line of polarity reversal; light blue circles, type II hair cells in zone 3; dark blue circles, type I hair cells in zone 3; light blue line, linear MM regression fit showing dependence of type II bundles on position within the striola (zones 2 and 3); red line, linear MM fit showing dependence of type I bundles on position within zone 3. Regression equations are shown at lower left for each fit with the associated probability that the slope of the regression line is different from 0. Bundle dimensions in and near the striola exhibit much more spatial variability than those in mid- to far-lateral (far left in scatter plots) and medial (Fig. 4) extrastriola. Box plots show differences between type I (left) and type II (right) bundles within zone 3. Plotting conventions are the same as in Fig. 4. Nonoverlapping confidence intervals and P values for Kolmogorov-Smirnov (ks) tests indicate that the two hair cell types differ significantly in height of the tallest stereocilia (B), KS ratio (C), array length (E), and bundle slope (F).

analysis. The problem is particularly acute in the striola, where there are few bundles in a single utricular slice. We attempted to circumvent this difficulty by collecting additional measurements from striolar bundles in adjacent sections, but large differences in sample sizes from different zones remain. This is one reason we used robust statistical methods for our analyses (Wilcox 2001).

The third criterion is known location. Most previous efforts to quantify bundle heights have used dissociated hair cells

(Ricci et al. 1997) or specified bundle locations very generally (e.g., striola versus extrastriola) or not at all. These studies present valuable overviews of bundle structure, but they can provide little insight on how or whether differences in bundle heights may contribute to regional differences in vestibular afferent physiology. We specified the location of each bundle relative to the line of polarity reversal. This yields a continuous ratio scale of location and thus more powerful options for

TABLE 1. *Samples for height measurements: number of measured bundles*

	n	Type II				Type I	
		Zone 1	Zone 2	Zone 3	Zone 4	All Zones	Zone 3
Primary							
<i>Turtle 2</i>	382	61	26	13	254	354	28
<i>Turtle 3</i>	423	80	9	5	307	401	22
Total	805	141	35	18	561	755	50
Posterior							
<i>Turtle 4</i>	202	33	8	5	148	194	8
<i>Turtle 5</i>	152	45	10	3	84	142	10
Total	354	78	18	8	232	336	18
Anterior							
<i>Turtle 4</i>	159	0	13	0	114	157	2
<i>Turtle 5</i>	371	108	29	15	201	353	18
Total	530	138	42	15	315	510	20
All transects	1689	357	95	41	1108	1601	88

Carapace lengths (inches): *turtle 2*, 5 1/8; *turtle 3*, 4 3/4; *turtle 4*, 4 3/4; *turtle 5*, 5 1/8.

statistical analysis (Zar 1999) than simply assigning bundles to discontinuous categories (e.g., striola versus extrastriola). To describe broad patterns of bundle structure, we also assigned bundles to utricular zones (Fig. 9). Zone 3 is defined as the band of type I hair cells and any intercalated type II hair cells. Zone 4 (the MES) is defined as the macular region medial to zone 3. At present, we define zone 2 as the band of hair cells between zone 3 and the line of polarity reversal; zone 1 (LES) comprises all hair cells lateral to the reversal line. As noted in the preceding text, a few hair cells lateral to the reversal line share features with zone 2 hair cells: short kinocilia, KS ratios ~ 1 , and calretinin-negative somata (Xue et al. 2005). These cells may properly belong to zone 2, i.e., to the striola. A broader, more vexed issue is how to define the striola. At present, our operational definition is that zones 2 and 3 collectively form the striola. Ideally, one would like a definition that is applicable to all vertebrates and does not depend on struc-

TABLE 2. *Kinocilium height*

	Type 2				Type I	
	Zone 1	Zone 2	Zone 3	Zone 4	All Zones	Zone 3
Primary transect						
Median	15.60	8.80	10.15	14.30	14.30	10.30
Interquartile range	4.70	1.00	3.10	3.90	4.30	3.10
Range	3.7–57.4	5.5–10.9	7.4–16.6	4.6–32.3	3.7–57.4	7.4–14.0
95% Confidence intervals of median	14.98–16.22	8.53–9.07	9.00–11.30	14.04–14.56	14.05–14.55	9.61–10.99
Posterior transect						
Median	15.75	9.10	9.80	13.80	13.75	10.45
Interquartile range	6.50	0.60	1.65	3.30	4.35	1.50
Range	4.3–35.0	7.9–10.5	8.1–12.3	2.3–37.7	2.3–37.7	8.5–14.8
95% Confidence intervals of median	14.59–16.91	8.88–9.32	8.88–10.72	13.46–14.14	13.38–14.12	9.89–11.01
Anterior transect						
Median	12.70	9.30	10.80	11.90	11.70	11.40
Interquartile range	4.20	1.20	2.10	2.90	3.40	0.60
Range	4.6–20.1	6.6–11.0	7.4–13.0	3.4–25.4	3.4–25.4	9.4–12.9
95% Confidence intervals of median	12.14–13.26	9.01–9.59	9.95–11.65	11.64–12.16	11.46–11.94	11.19–11.61
All transects						
Median	14.50	9.10	10.30	13.40	13.30	10.80
Interquartile range	5.20	1.00	2.30	3.90	4.60	2.50
Range	3.7–57.4	5.5–11.0	7.4–16.6	2.3–37.7	2.3–57.4	7.4–14.8
95% Confidence intervals of median	14.07–14.93	8.94–9.26	9.73–10.87	13.22–13.58	13.12–13.48	10.38–11.22

Height in μm .

tural or physiological details specific to individual species or taxa. Whether this is possible remains to be established.

The fourth criterion is accurate identification of hair cell type. We identified type I hair cells by the presence of a calyx, which we labeled with Micro-Ruby applied to the utricular nerve. We discussed the potential limitations of this method previously and our reasons for concluding that the number of misidentified type I hair cells, if any, must be small (Moravec and Peterson 2004, p. 3158). Recently, we have identified type I hair cells by labeling calyces with calretinin and/or β -III tubulin; the resulting type-specific differences in bundle heights (Xue et al. 2005) are essentially identical to those in the present study. For example, the ratio of type I/type II dimensions on all six variables in the current study (Fig. 6) differed from results of Xue et al. (2005) by an average of 0.04.

Relation to previous work

Two previous studies compared heights of identified type I and type II bundles in vestibular organs. Using scanning micrographs of fractured guinea pig saccules, Lapeyre et al. (1992) reported that the tallest stereocilia of type I bundles are taller than those of type II bundles on average and unlike type II bundles, they vary with macular locus. Ricci et al. (1997) concluded that bundle (apparently kinocilium) heights of type I hair cells in pigeon are shorter, on average than those of type II hair cells when vestibular end organs are considered as a group. This was partly due to a subpopulation of type I hair cells with short bundles.

More information is available about height variation in type II hair bundles. Building on an earlier classification (Baird and Lewis 1986; Lewis and Li 1975) Baird used light microscopy to measure kinocilia and stereocilia heights of the four bundle types found in bullfrog utricle (Baird 1994a,b). His results are very similar to ours: KS ratios are highest in the extrastriola and decline systematically toward the line of polarity reversal. Bundle heights of type II hair cells from otolith organs have

TABLE 3. *Height of tallest stereocilia*

	Type II					Type I
	Zone 1	Zone 2	Zone 3	Zone 4	All Zones	Zone 3
Primary transect						
Median	5.70	9.20	4.35	3.80	4.10	7.30
Interquartile range	3.80	1.70	1.40	1.20	1.60	2.10
Range	2.1–27.9	6.1–11.4	2.8–5.9	1.9–8.5	1.9–27.9	3.9–11.7
95% Confidence intervals of median	5.20–6.20	8.75–9.65	3.83–4.87	3.72–3.88	4.01–4.19	6.83–7.77
Posterior transect						
Median	4.70	8.60	4.65	4.50	4.60	8.00
Interquartile range	2.40	1.50	1.75	1.45	1.80	1.20
Range	2.5–17.6	6.4–11.2	3.3–7.3	2.7–10.5	2.5–17.6	6.1–10.8
95% Confidence intervals of median	4.27–5.13	8.04–9.16	3.68–5.62	4.35–4.65	4.45–4.75	7.55–8.45
Anterior transect						
Median	5.60	8.30	4.10	3.70	4.20	7.70
Interquartile range	3.60	2.20	1.70	0.90	2.00	2.45
Range	2.2–12.3	3.7–11.4	2.6–5.8	2.5–8.4	2.2–12.3	3.3–11.7
95% Confidence intervals of median	5.12–6.08	7.77–8.83	3.41–4.79	3.62–3.78	4.06–4.34	6.84–8.56
All transects						
Median	5.50	8.70	4.30	3.90	4.20	7.60
Interquartile range	3.40	1.70	1.70	1.20	2.00	1.90
Range	2.1–27.9	3.7–11.4	2.6–7.3	1.9–10.5	1.9–27.9	3.3–11.7
95% Confidence intervals of median	5.22–5.78	8.43–8.97	3.88–4.72	3.84–3.96	4.12–4.28	7.28–7.92

been described in many publications (reviews: Eatock and Lysakowski 2005; Lewis et al. 1985; Platt 1983; Smotherman and Narins 2000), but patterns are hard to discern for three reasons. First, many papers report heights of “bundles” without specifying whether the measurements were of kinocilia or stereocilia. Second, many descriptions are qualitative in whole or in part. For example, they report numbers for stereocilia heights and refer to kinocilia as “long” or “longer.” Third, most reports include little or no locational information. One exception is Platt and Popper (1984), who quantified spatial patterns in saccular bundle heights of two teleosts.

Review of this literature suggests three broad conclusions about the heights of type II bundles. First, utricular bundle heights are roughly similar to bundle heights in other otolith organs and shorter than bundles in the semicircular canals. Second, bundle heights depend on utricular locus in all verte-

brate classes: KS ratios in the striola or “central” region tend to be lower than in the extrastriola or “periphery.” Third, within a given region subgroups are sometimes identified based on KS ratios. Our results are consistent with these conclusions: KS ratios are lower in the striola than in the extrastriola (Figs. 4, 6, and 8) and within the striola KS ratios for type II bundles differ significantly between zones 2 and 3 (Figs. 6–8).

Variability in bundle heights has led to a number of classification schemes, most notably the Fx and K_{xsx} classifications of fish bundles by Popper (1977) and Platt (1983), respectively, the A-E classification of frog bundles by Lewis and Li (1975), and the P_x/S_x classification of mammalian bundles by Lim (1976). Probable correspondences between bundle classes in anamniotes are reviewed in Platt (1983). In the present study, we have not assigned bundles to classes based on kinocilium and/or stereocilia heights. This might be reasonable for ho-

TABLE 4. *KS ratio*

	Type II					Type I
	Zone 1	Zone 2	Zone 3	Zone 4	All Zones	Zone 3
Primary transect						
Median	2.93	0.99	2.41	3.77	3.52	1.47
Interquartile range	1.39	0.20	0.69	1.28	1.51	0.53
Range	0.4–6.3	0.6–1.6	1.7–4.2	1.2–7.7	0.4–7.7	0.8–3.5
95% Confidence intervals of median	2.74–3.11	0.94–1.04	2.16–2.67	3.68–3.85	3.44–3.61	1.36–1.59
Posterior transect						
Median	3.15	1.06	1.98	3.12	3.07	1.28
Interquartile range	1.43	0.19	1.10	0.84	1.10	0.29
Range	0.9–5.9	0.8–1.5	1.4–3.4	0.8–6.5	0.8–6.5	0.9–1.8
95% Confidence intervals of median	2.89–3.40	0.99–1.14	1.36–2.59	3.03–3.20	2.97–3.16	1.18–1.39
Anterior transect						
Median	2.34	1.10	2.37	3.15	2.89	1.42
Interquartile range	1.50	0.22	1.25	0.68	1.30	0.60
Range	0.8–4.1	0.8–2.2	1.8–4.8	1.1–5.5	0.8–5.5	1.0–3.5
95% Confidence intervals of median	2.14–2.54	1.04–1.15	1.86–2.88	3.09–3.21	2.80–2.98	1.20–1.63
All transects						
Median	2.75	1.07	2.34	3.35	3.16	1.42
Interquartile range	1.55	0.21	0.93	1.09	1.33	0.51
Range	0.4–6.3	0.6–2.2	1.4–4.3	0.8–7.7	0.4–7.7	0.8–3.5
95% Confidence intervals of median	2.63–2.88	1.03–1.10	2.11–2.57	3.30–3.40	3.10–3.21	1.33–1.50

TABLE 5. *Height of shortest stereocilia*

	Type II					Type I
	Zone 1	Zone 2	Zone 3	Zone 4	All Zones	Zone 3
Primary transect						
Median	1.30	2.00	1.40	1.50	1.40	1.50
Interquartile range	0.50	0.80	0.50	0.30	0.40	0.60
Range	0.6–3.5	1.1–3.2	0.9–2.0	0.6–2.6	0.6–3.5	0.9–2.7
95% Confidence intervals of median	1.23–3.67	1.79–2.21	1.21–1.59	1.48–1.52	1.38–1.42	1.37–1.63
Posterior transect						
Median	1.20	1.90	1.20	1.50	1.40	1.55
Interquartile range	0.50	0.50	0.55	0.55	0.60	0.50
Range	0.6–3.5	1.2–2.8	0.8–1.7	0.5–2.9	0.5–3.5	1.1–2.1
95% Confidence intervals of median	1.11–1.29	1.71–2.09	0.89–1.51	1.44–1.56	1.35–1.45	1.36–1.74
Anterior transect						
Median	1.40	2.15	1.20	1.40	1.40	1.80
Interquartile range	0.70	0.80	0.30	0.50	0.60	0.60
Range	0.6–4.7	0.9–3.5	0.9–1.6	0.6–2.5	0.6–4.7	1.0–2.5
95% Confidence intervals of median	1.31–1.49	1.96–2.34	1.08–1.32	1.36–1.44	1.36–1.44	1.59–2.01
All transects						
Median	1.30	2.00	1.30	1.40	1.40	1.60
Interquartile range	0.60	0.80	0.40	0.50	0.50	0.60
Range	0.6–4.7	0.9–3.5	0.8–2.0	0.5–2.9	0.5–4.7	0.9–2.7
95% Confidence intervals of median	1.25–1.35	1.87–2.13	1.20–1.40	1.38–1.42	1.38–1.42	1.50–1.70

Height in μm .

homogeneous bundle populations (e.g., in striolar zone 2), but it would be inappropriate for bundles in striolar zone 3 and the lateral extrastriola (zone 1) where there are considerable variability and clear spatial gradients in bundle heights. Instead, we use a spatial framework to organize variability in bundle heights, i.e., we describe heights as a function of location along a radial transect through the utricular macula. We defer attempts to classify bundles until we know more about their functional roles. One advantage of organizing height information by location is that it facilitates comparisons between properties of hair bundles and utricular afferents, which also vary as a function of utricular locus (see *Relation to afferent physiology*).

TABLE 6. *Array length*

	Type II					Type I
	Zone 1	Zone 2	Zone 3	Zone 4	All Zones	Zone 3
Primary transect						
Median	2.50	3.40	2.70	4.00	3.80	3.60
Interquartile range	0.80	1.10	0.50	0.90	1.20	0.80
Range	1.3–5.2	1.5–4.6	1.7–4.2	1.9–6.3	1.3–6.3	2.3–4.6
95% Confidence intervals of median	2.39–2.61	3.11–3.69	2.51–2.89	3.94–4.06	3.73–3.87	3.42–3.78
Posterior transect						
Median	2.50	3.10	2.65	3.80	3.50	3.60
Interquartile range	0.70	0.70	0.75	0.85	1.20	0.70
Range	1.3–3.8	2.1–4.8	1.8–3.7	1.9–7.6	1.3–7.6	3.0–5.2
95% Confidence intervals of median	2.38–2.62	2.84–3.36	2.23–3.07	3.71–3.89	3.40–3.60	3.34–3.86
Anterior transect						
Median	2.50	3.30	2.60	3.80	3.30	3.60
Interquartile range	0.50	0.80	0.50	1.00	1.20	0.70
Range	1.4–4.5	1.7–5.0	1.5–3.2	1.3–6.0	1.3–6.0	2.2–4.9
95% Confidence intervals of median	2.43–2.57	3.11–3.49	2.40–2.80	3.71–3.89	3.22–3.38	3.35–3.85
All transects						
Median	2.50	3.30	2.70	3.90	3.60	3.60
Interquartile range	0.70	0.90	0.50	0.90	1.20	0.70
Range	1.3–5.2	1.5–5.0	1.5–4.2	1.3–7.6	1.3–7.6	2.2–5.2
95% Confidence intervals of median	2.44–2.56	3.15–3.45	2.58–2.82	3.86–3.94	3.55–3.65	3.48–3.72

Length in μm .

Functional significance of bundle heights

Experiments and models suggest that bundle heights affect several aspects of bundle performance. First is frequency selectivity. Variation in stereocilia heights confers frequency selectivity on free-standing auditory hair cells of certain lizards (review: Aranyosi and Freeman 2004). Interestingly, bundle heights are correlated with best frequencies in many additional amniote hearing organs (cochlea or basilar papilla) (Saunders and Dear 1983), but in these species (Fettiplace and Fuchs 1999) and in frog auditory organs (Smotherman and Narins 2000), height variation alone probably does not account for frequency selectivity.

TABLE 7. *Slope*

	Type II					Type I
	Zone 1	Zone 2	Zone 3	Zone 4	All Zones	Zone 3
Primary transect						
Median	1.78	2.08	1.14	0.56	0.69	1.52
Interquartile range	1.61	0.50	0.29	0.32	0.75	0.61
Range	0.4–10.2	1.4–3.9	0.4–1.9	0.1–2.5	0.1–10.2	0.8–2.6
95% Confidence intervals of median	1.56–1.99	1.95–2.21	1.03–1.24	0.54–0.58	0.65–0.74	1.39–1.66
Posterior transect						
Median	1.33	2.12	1.47	0.75	0.89	1.73
Interquartile range	1.06	0.74	0.53	0.38	0.67	0.42
Range	0.7–4.8	1.4–3.6	0.9–1.9	0.4–2.7	0.4–4.8	1.4–2.4
95% Confidence intervals of median	1.14–1.52	1.84–2.39	1.18–1.76	0.71–0.79	0.84–0.95	1.57–1.88
Anterior transect						
Median	1.64	1.94	1.08	0.66	0.85	1.49
Interquartile range	1.13	0.61	0.58	0.31	0.93	0.51
Range	0.3–4.6	0.7–3.4	0.5–1.7	0.3–2.5	0.3–4.6	0.8–2.3
95% Confidence intervals of median	1.49–1.79	1.79–2.09	0.84–1.31	0.63–0.68	0.79–0.92	1.31–1.67
All transects						
Median	1.63	2.00	1.15	0.64	0.77	1.54
Interquartile range	1.25	0.61	0.47	0.34	0.79	0.53
Range	0.3–10.2	0.7–3.9	0.4–1.9	0.1–2.7	0.1–10.2	0.8–2.6
95% Confidence intervals of median	1.52–1.73	1.90–2.10	1.03–1.27	0.63–0.66	0.74–0.80	1.45–1.63

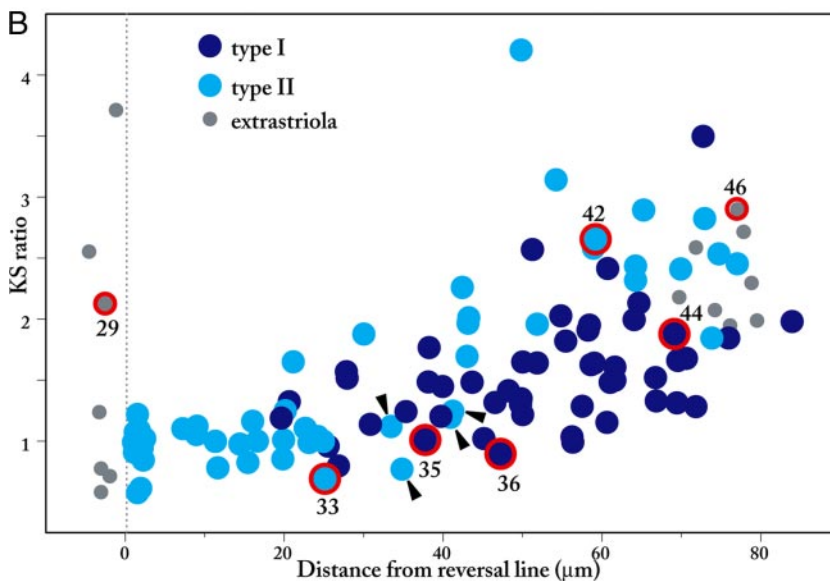
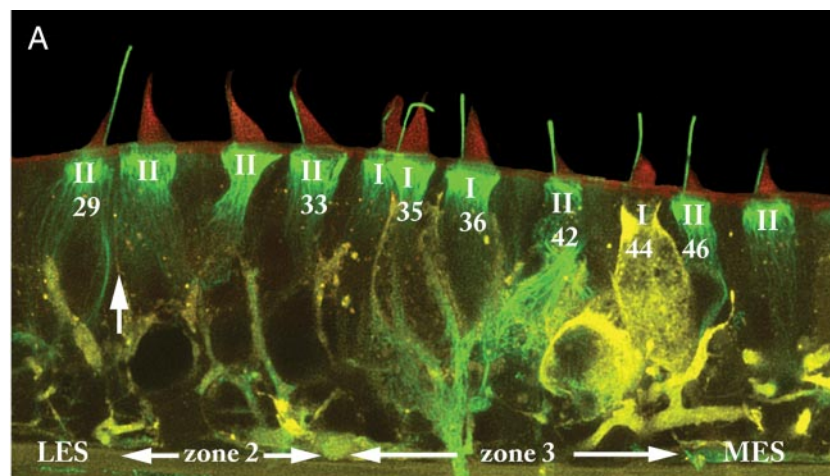


FIG. 7. Spatial- and type-specific variation in KS ratios of striolar bundles. *A*: confocal projection showing the striola and adjacent LES and MES. Staining is the same as in Fig. 2. The micrograph is from a slightly different level of the confocal stack shown in Fig. 2*B*. The image was enhanced using deconvolution (Autoquant). Arrow: line of polarity reversal. I, type I hair cell; II, type II hair cell. Numbered hair cells correspond to circled data points in *B*. *B*: KS ratio changes with distance from the reversal line (0). This plot shows details of region- and type-specific differences in KS ratios within the striola; data points are taken from the striolar region of Figs. 4*C* and 6*C*. The plot is aligned with the micrograph in *A*. Light blue circles, type II hair cells in the striola; dark blue circles, type I hair cells in zone 3; gray circles, type II hair cells in extrastriola. Zone 2 contains a homogeneous population of type II bundles. Arrowheads mark four type II bundles in zone 2; they appear to overlap zone 3 because the line separating the two striolar zones is irregular. In zone 3, KS ratios of both hair cell types increase with distance from the reversal line, but at each position within zone 3 KS ratios are generally lower for type I than for type II receptors. Red circles around data points mark numbered bundles in *A*.

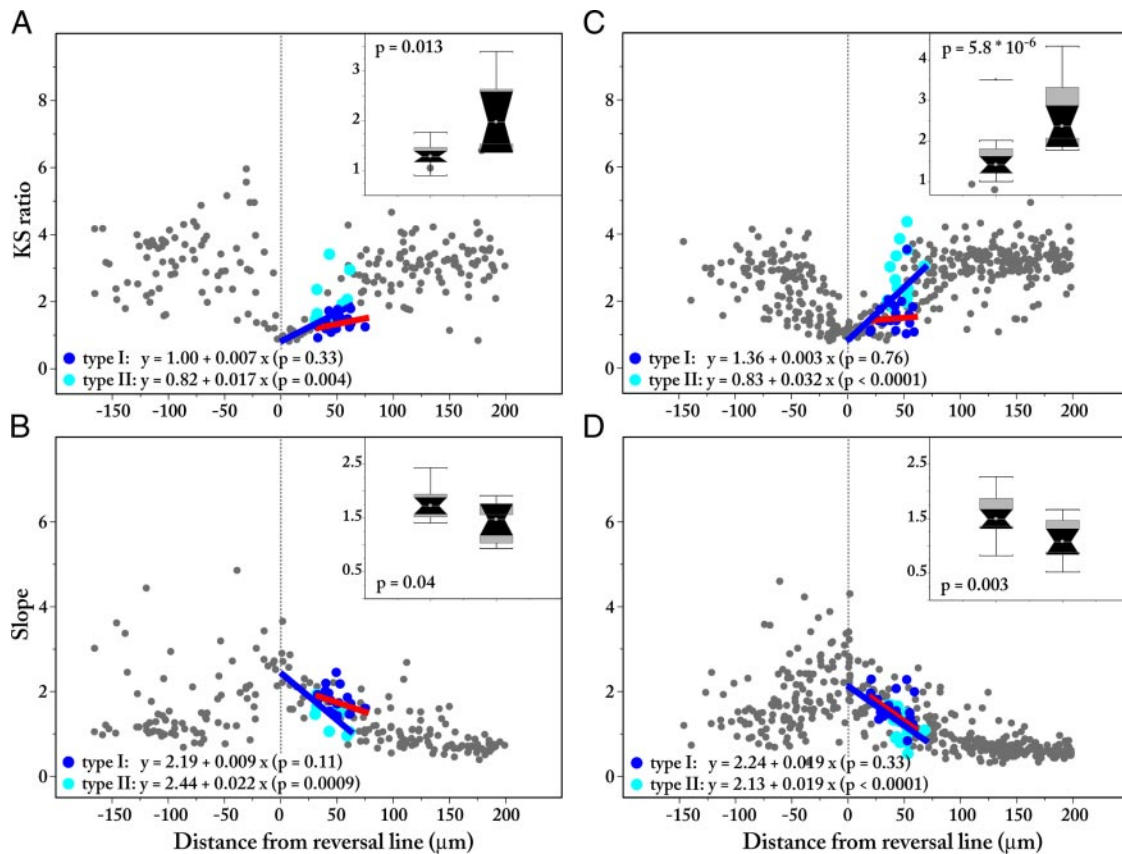


FIG. 8. Spatial- and type-specific variation in posterior and anterior striola. Scatter plots show changes in KS ratio (A and C) and bundle slope (B and D) in and near the striola for posterior (A and B) and anterior (C and D) transects. Additional measures for the 2 transects are summarized in Tables 2–7. Each symbol represents 1 hair bundle. Dark gray circles, bundles $\pm 200 \mu\text{m}$ from the line of polarity reversal; light blue circles, type II hair cells in zone 3; dark blue circles, type I hair cells in zone 3. Box plots show differences between type I (left) and type II (right) bundles within zone 3 and P values for ks tests; plotting conventions are the same as in Fig. 4. These type-specific differences in KS ratio and bundle slope are comparable to those observed in the primary transect (Fig. 6, C and F).

Second, operating range, defined as the tip displacement required to produce 90% of the hair cell response, is positively related to bundle height in bullfrog (Baird 1994b) and mouse (Géléoc et al. 1997). Taller bundles can be displaced further than shorter bundles before the hair cell response saturates; thus they can monitor a wider range of displacements. This suggests that the tall bundles in medial or lateral extrastriola of turtle utricle may have larger operating ranges than those in the striola.

Third, sensitivity, defined as the slope of the response-displacement curve, is inversely related to bundle height (Baird 1994b; Géléoc et al. 1997). Two explanations have been suggested. First, geometry dictates that a unit displacement of a bundle's tip will result in a smaller angular rotation of a tall bundle than of a short bundle. Smaller rotation of the tall bundle translates into lower tensions on mechanotransduction channels and lower open channel probability. Thus the magnitude of the transduction current in response to a given deflection (sensitivity) will depend in part on the height of the bundle tip (usually the kinocilium tip) above the epithelium (Jacobs and Hudspeth 1990). Second, experiments and models in bullfrog utricle led Baird (1994b) to suggest that KS ratio may be an even more important geometric factor: shorter stereocilia undergo relatively small displacements when a force is applied to a much longer kinocilium. These geometric analyses assume that the kinocilium and stereocilia in the bundle undergo equal angular rotations, which may (Corey et

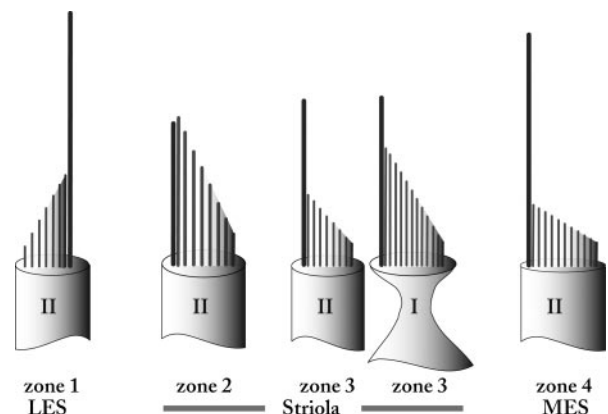


FIG. 9. Hair bundle heights in turtle utricle. Scale drawings of 5 bundle morphologies in turtle utricle. The drawings depict median values for kinocilium height, heights of tallest and shortest stereocilia, and array length (Tables 2–7). At present, we assume a linear decrease in bundle heights. The median structure of type II hair cells (II) varies significantly with utricular zone. Drawings for type II bundles in striolar zone 2 and zone 4 (medial extrastriola; MES) are good approximations of all bundles in the respective zones because these two populations are relatively homogeneous. The drawing for type II bundles in zone 1 (lateral extrastriola; LES) is typical of hair cells $>30 \mu\text{m}$ lateral to the reversal line; closer to the reversal line, the kinocilia and tallest stereocilia of some zone 1 bundles are much longer than are depicted in the diagram (Fig. 6, A and B). The drawings for type I (I) and type II bundles in striolar zone 3 reflect median differences in KS ratio and array length; absolute KS ratios for both bundle types can vary with position in zone 3 (Fig. 7).

al. 1989; MacDonald and Corey 1996) or may not (Duncan et al. 1995; Eisen et al. 1999) be the case. Furthermore, other factors may contribute to tensions on transduction channels, e.g., inter-stereocilia spacing (Jacobs and Hudspeth 1990), or affect the magnitude of the transduction current (e.g., stereocilia number, number of channels per stereocilium, and variations in single-channel conductance) (see discussion in Moravec and Peterson 2004). Nevertheless, bundle height is one important determinant of a vestibular hair cell's response to displacement. Based on these considerations, we expect that striolar bundles in turtle utricle, which are short and have low KS ratios, will be more sensitive to displacement than extrastriolar bundles. Similarly, type I hair cells with their low KS ratios may have greater sensitivities than type II hair cells in the same striolar zone.

Fourth is stiffness. Bundle heights affect bundle stiffness in two ways. First, the translational stiffness of a bundle is inversely proportional to the square of the height at which force is applied. This well-known relationship (Howard et al. 1988) has been demonstrated experimentally in bullfrogs (Howard and Ashmore 1986) and mice (Géléoc et al. 1997). Thus if force is applied to the kinocilium tip, bundles with short kinocilia will present a higher translational stiffness than those with tall kinocilia. Second, the relative heights of kinocilia and stereocilia have important effects on bundle stiffness. Any two linked elements of different heights (e.g., the kinocilium and the tallest stereocilium or 2 stereocilia of different heights) can be thought of as a (class 2) lever system. The mechanical advantage of a force acting on the taller element (its ability to deflect the shorter element) depends on the ratio of their heights. For example, bundles with large KS ratios will resist deflection less because the mechanical advantage of the kinocilium is high. Finite-element models (Silber et al. 2004) and correlated height and stiffness measurements on turtle utricular bundles using calibrated flexible probes (Moravec et al. 2005; Spoon et al. 2005) both support the suggestion that KS ratio is an important determinant of bundle stiffness. Stiffness is greatest in zone 2, where KS ratios are ~ 1 , and it declines systematically through zone 3 to reach asymptotic, low values in zone 4. Thus measured bundle stiffness shows a striking inverse relationship to KS ratio (cf. Fig. 4C). Other factors may contribute to bundle stiffness (e.g., stereocilia number or the type and number of interstereociliary links). Interestingly, our experiments suggest that bundle height (KS ratio) has a greater effect on bundle stiffness than stereocilia number: most bundles in striolar zone 3 have significantly more stereocilia than those in zone 2 (Moravec and Peterson 2004), yet they are more compliant.

The fifth aspect of bundle performance is response phase. Utricular bundles are deflected by displacement of the otocorial membrane (OM) to which they are attached (point loading), and by endolymph flow (fluid loading). OM displacement is in phase with head acceleration; endolymph flow is in phase with jerk (Grant and Best 1987). The relative effectiveness of these two loading regimens depends in part on stereocilia heights. For example, striolar bundles are unique because they have tall stereocilia (Fig. 4B) and they are wide (E. H. Peterson and M. H. Rowe, unpublished data). Thus they present a larger area to endolymph flow than do extrastriolar bundles and are subject to greater fluid drag. Our finite-element models suggest that, as a result, fluid forcing has a greater effect on striolar

bundles than on extrastriolar bundles. Thus the response of striolar bundles is more likely to be phase advanced toward jerk (Nam et al. 2005). The relatively steep height gradient of striolar bundles (slope; Fig. 4F) contributes to this phase advance (Kondrachuk 2002; Nam et al. 2005). One interesting possibility is that this effect, which is partly a result of stereocilia heights, may contribute to a phase advance in afferents innervating the striola such as that reported in chinchilla utricle (Goldberg et al. 1990).

Relation to utricular afferent physiology

The single best predictor of afferent physiological profiles is location on the neuroepithelium. This is true of canals (Baird et al. 1988; Boyle et al. 1991; Brichta and Goldberg 2000a,b; Honrubia et al. 1989; Myers and Lewis 1990, 1991; Schessel et al. 1991) and of otolith organs (Baird and Lewis 1986; Goldberg et al. 1990). The most common observation is that physiological profiles of central or striolar afferents differ from those of the periphery or extrastriola. Several of these studies have also reported detailed peripheral-to-central gradients in afferent physiology. A number of candidate mechanisms have been proposed, including regional variation in hair cell transduction, synaptic mechanisms, and mechanics (reviews: Eatock and Lysakowski 2005; Goldberg 2000; Highstein et al. 2005; Lysakowski and Goldberg 2004; Rabbitt et al. 2004). Our results and the data available on other vestibular organs (see *Relation to previous work*) together suggest that bundle heights exhibit similar spatial patterns. As described in the preceding text, bundle heights affect bundle mechanics and hair cell transduction. Thus we suggest that location- and type-specific differences in bundle heights, such as those we describe here, will contribute to parallel differences in bundle mechanics, hair cell transduction, and ultimately, afferent responses to head movement.

ACKNOWLEDGMENTS

We thank Dr. Iain Miller for deconvolution of the confocal images in Figs. 2, B and C, and 7A. R.A. Eatock, J. W. Grant, M. H. Rowe, and J.-H. Nam provided helpful comments on the manuscript.

GRANTS

This work was supported by National Institute of Deafness and Other Communications Disorders Grant DC-05063 to E. H. Peterson.

REFERENCES

- Aranyosi AJ and Freeman DM. Sound-induced motions of individual cochlear hair bundles. *Biophys J* 87: 3536–3546, 2004.
- Baird RA. Comparative transduction mechanisms of hair cells in the bullfrog utricle. I. Responses to intracellular current. *J Neurophysiol* 71: 666–684, 1994a.
- Baird RA. Comparative transduction mechanisms of hair cells in the bullfrog utricle. II. Sensitivity and response dynamics to hair bundle displacement. *J Neurophysiol* 71: 685–705, 1994b.
- Baird RA, Desmadryl G, Fernandez C, and Goldberg JM. The vestibular nerve of the chinchilla. II. Relation between afferent response properties and peripheral innervation patterns in the semicircular canals. *J Neurophysiol* 60: 182–203, 1988.
- Baird RA and Lewis ER. Correspondences between afferent innervation patterns and response dynamics in the bullfrog utricle and lagena. *Brain Res* 369: 48–64, 1986.
- Boyle R, Carey JP, and Highstein SM. Morphological correlates of response dynamics and efferent stimulation in horizontal semicircular canal afferents of the toadfish, *Opsanus tau*. *J Neurophysiol* 66: 1504–1521, 1991.

- Brichta AM and Goldberg JM.** Morphological identification of physiologically characterized afferents innervating the turtle posterior crista. *J Neurophysiol* 83: 1202–1223, 2000a.
- Brichta AM and Goldberg JM.** Responses to efferent activation and excitatory response-intensity relations of turtle posterior-crista afferents. *J Neurophysiol* 83: 1224–1242, 2000b.
- Brichta AM and Peterson EH.** Functional architecture of vestibular primary afferents from the posterior semicircular canal of a turtle, *Pseudemys (Trachemys) scripta elegans*. *J Comp Neurol* 344: 481–507, 1994.
- Cleveland WS.** *Visualizing data*. Summit, NJ: Hobart, 1993.
- Corey DP, Huang PL, and Assad JA.** Hair cell stereocilia bend at their bases and touch at their tips. *Soc Neurosci Abstr* 15: 208, 1989.
- Crawford AC, Evans MG, and Fettiplace R.** The actions of calcium on the mechano-electrical transducer current of turtle hair cells. *J Physiol* 434: 369–398, 1991.
- Duncan RK, Hernandez HN, and Saunders JC.** Relative stereocilia motion of chick cochlear hair cells during high-frequency water-jet stimulation. *Audit Neurosci* 1: 321–329, 1995.
- Eatock RA and Lysakowski A.** Mammalian vestibular hair cells. In: *Vertebrate Hair Cells*, edited by RA Eatock, AN Popper, and RR Fay. New York: Springer-Verlag, 2006, p. 348–442.
- Edge RM, Evans BN, Pearce M, Richter C-P, Hu X, and Dallos P.** Morphology of the unfixed cochlea. *Hear Res* 124: 1–16, 1998.
- Eisen MD, Duncan RK, and Saunders JC.** The tip link's role in asymmetric stereocilia motion of chick cochlear hair cells. *Hear Res* 127: 14–21, 1999.
- Emerson JD and Strenio J.** Boxplots and batch comparison. In: *Understanding Robust and Exploratory Data Analysis*, edited by DC Hoaglin, F Mosteller, and JW Tukey. New York: Wiley, 1983, p. 58–96.
- Fettiplace R and Fuchs PA.** Mechanisms of hair cell tuning. *Annu Rev Physiol* 61: 809–834, 1999.
- Fontilla MF and Peterson EH.** Kinocilia heights on utricular hair cells. *Hear Res* 145: 8–16, 2000.
- Freeman DM, Hendrix DK, Shah D, Fran LF, and Weiss TF.** Effect of lymph composition on an in vitro preparation of the alligator lizard cochlea. *Hear Res* 65: 83–98, 1993.
- Géléoc GSG, Lennan GWT, Richardson GP, and Kros CJ.** A quantitative comparison of mechano-electrical transduction in vestibular and auditory hair cells of neonatal mice. *Proc R Soc Lond B Biol Sci* 264: 611–621, 1997.
- Goldberg JM.** Afferent diversity and the organization of central vestibular pathways. *Exp Brain Res* 130: 277–297, 2000.
- Goldberg JM, Desmadryl G, Baird RA, and Fernandez C.** The vestibular nerve of the chinchilla. V. Relation between afferent discharge properties and peripheral innervation patterns in the utricular macula. *J Neurophysiol* 63: 791–804, 1990.
- Grant JW and Best W.** Otolith-organ mechanics: lumped parameter model and dynamic response. *Aviat Space Environ Med* 58: 970–976, 1987.
- Highstein SM, Rabbitt RD, Holstein GR, and Boyle RD.** Determinants of spatial and temporal coding by semicircular canal afferents. *J Neurophysiol* 93: 2359–2370, 2005.
- Honrubia V, Hoffman LF, Sitko S, and Schwartz IR.** Anatomic and physiological correlates in bullfrog vestibular nerve. *J Neurophysiol* 61: 688–701, 1989.
- Houngaard J and Nicholson C.** The isolated turtle brain and the physiology of neuronal circuits. In: *Preparations of Vertebrate Central Nervous System In Vitro*, edited by Jahnsen H. London: Wiley, 1990, p. 155–181.
- Howard J and Ashmore JF.** Stiffness of sensory hair bundles in the sacculus of the frog. *Hear Res* 23: 93–104, 1986.
- Howard J, Roberts WM, and Hudspeth AJ.** Mechano-electrical transduction by hair cells. *Annu Rev Biophys Chem* 17: 99–124, 1988.
- Jacobs RA and Hudspeth AJ.** Ultrastructural correlates of mechano-electrical transduction in hair cells of the bullfrog's internal ear. *Cold Spring Harbor Symp Quant Biol* 55: 547–562, 1990.
- Jorgensen JM.** The sensory epithelia of the inner ear of two turtles, *Testudo graeca L.* and *Pseudemys scripta*. *Acta Zool* 55: 289–298, 1974.
- Jorgensen JM.** The number and distribution of calyceal hair cells in the inner ear utricular macula of some reptiles. *Acta Zool* 69: 169–175, 1988.
- Kondrachuk AV.** Models of otolithic membrane-hair cell bundle interaction. *Hear Res* 166: 96–112, 2002.
- Lapeyre P, Guilhaume A, and Cazals Y.** Differences in hair bundles associated with type-I and type-II vestibular hair cells of the guinea pig sacculle. *Acta Otolaryngol* 112: 635–642, 1992.
- Lewis ER and Li CW.** Hair cell types and distributions in the otolithic and auditory organs of the bullfrog. *Brain Res* 83: 35–50, 1975.
- Lewis ER, Leverenz EL, and Bialek WS.** Comparative inner ear anatomy. In: *The Vertebrate Inner Ear*, Boca Raton, FL: CRC, 1985, p. 66–73.
- Lim DJ.** Morphological and physiological correlates in cochlear and vestibular sensory epithelia. *Scan Elec Micro V* 269–276, 1976.
- Lysakowski A and Goldberg JM.** Morphophysiology of the vestibular periphery. In: *The Vestibular System*, edited by Highstein SM, Fay RR, and Popper AN. New York: Springer, 2004, p. 57–152.
- MacDonald RB and Corey DP.** Stereocilia bundles of the bullfrog sacculus hair cells do not splay in response to stimulation. *Assoc Res Otolaryngol Abstr* 1919: 60, 1996.
- Moravec WJ and Peterson EH.** Differences between stereocilia numbers on type I and type II vestibular hair cells. *J Neurophysiol* 92: 3153–3160, 2004.
- Moravec WJ, Xue J, Rowe MH and Peterson EH.** Hair bundles of the utricular striola in a turtle, *Trachemys scripta*. *Assoc Res Otolaryngol Abstr* 26: 33, 2003.
- Moravec WJ, Spoon C, Grant JW, and Peterson EH.** Bundle mechanics depend on bundle structure II: using artificial neural networks to perform non-linear statistical analyses. *Soc Neurosci Abstr* 471.1, 2005.
- Myers SF and Lewis ER.** Hair cell tufts and afferent innervation of the bullfrog crista-ampullaris. *Brain Res* 534: 15–24, 1990.
- Myers SF and Lewis ER.** Vestibular afferent responses to microrotational stimuli. *Brain Res* 542: 36–44, 1991.
- Nam J-H, Cotton JR, Peterson EH, and Grant JW.** 2005 Computational analysis of the effects of hair bundle shape and loading condition on mechanotransduction. *Soc Neurosci Abstr*, 47.3, 2005.
- O'Leary DP, Dunn RF, and Honrubia V.** Analysis of afferent responses from isolated semicircular canal of the guitarfish using rotational acceleration white-noise inputs. I. Correlation of response dynamics with receptor innervation. *J Neurophysiol* 39: 631–644, 1976.
- Peterson EH.** Are there parallel channels in the vestibular nerve? *News Physiol Sci* 13: 194–201, 1998.
- Peterson EH and Rowe MH.** Autocorrelation analysis of stereociliary arrays on utricular hair cells. *Soc Neurosci Abstr* 27: 298.22, 2001.
- Platt C.** The peripheral vestibular system of fishes. In: *Fish Neurobiology*, edited by Northcutt RG and Davis RE. Ann Arbor, MI: Univ. of Michigan Press, 1983, p. 89–123.
- Platt C and Popper AN.** Variation in lengths of ciliary bundles on hair cells along the macula of the sacculus in two species of teleost fishes. *Scan Elec Micro IV* 1915–1924, 1984.
- Popper AN.** A scanning electron microscopic study of the sacculus and lagena in the ears of fifteen species of teleost fishes. *J Morphol* 153: 397–418, 1977.
- Rabbitt RD, Damiano ER, and Grant JW.** Biomechanics of the semicircular canals and otolith organs. In: *The Vestibular System*, edited by Highstein SM, Fay RR, and Popper AN. New York: Springer, 2004, p. 153–201.
- Ricci AJ, Cochran SL, Rennie KJ, and Correia MJ.** Vestibular type I and type II hair cells. II. Morphometric comparisons of dissociated pigeon hair cells. *J Vestib Res* 7: 407–420, 1997.
- Saunders JC and Dear SP.** Comparative morphology of stereocilia. In: *Hearing and Other Senses*, edited by Fay RR and Gourevitch G. Groton, CN: Amphora, 1983, p. 175–197.
- Schessel DA, Ginzberg R, and Highstein SM.** Morphophysiology of synaptic transmission between type I hair cells and vestibular primary afferents. An intracellular study employing horseradish peroxidase in the lizard, *Calotes versicolor*. *Brain Res* 544: 1–16, 1991.
- Severinsen SA, Jorgensen JM, and Nyegaard JR.** Structure and growth of the utricular macula in the inner ear of the slider turtle *Trachemys scripta*. *J Assoc Res Otolaryngol* 4: 505–520, 2003.
- Silber J, Cotton J, Nam J-H, Peterson EH, and Grant W.** Computational models of hair cell bundle mechanics. III. 3-D utricular bundles. *Hear Res* 197: 112–130, 2004.
- Smotherman MS and Narins PM.** Hair cells, hearing and hopping: a field guide to hair cell physiology in the frog. *J Exp Biol* 203: 2237–2246, 2000.
- Spoon C, Peterson E, and Grant JW.** Bundle mechanics depends on bundle structure in turtle utricle. *Assoc Res Otolaryngol Abstr* 28: 300, 2005.
- Xue J, Moravec W, and Peterson EH.** Differences between hair bundles of type I hair cells in turtle utricle. *Assoc Res Otolaryngol* 28: 300–301, 2005.
- Xue J and Peterson EH.** Organization of the utricular striola in *Trachemys scripta*: bundle heights. *Assoc Res Otolaryngol Abstr* 27: 318, 2004.
- Wilcox RR.** *Fundamentals of Modern Statistical Methods. Substantially Improving Power and Accuracy*. New York: Springer, 2001.
- Wilcox RR.** *Introduction to Robust Estimation and Hypothesis Testing*. Burlington, MA: Elsevier, 2005.
- Zar JH.** *Biostatistical Analysis*. Upper Saddle River, NJ: Prentice-Hall, 1999.